Journal of Science and Transport Technology
Journal homepage: https://jstt.vn/index.php/en

Mechanics-Aware Machine Learning Classification of Reinforced Concrete Shear Wall Failure Modes Using Dimensional and Non-Dimensional Features

Anh Le The[1], Chien Mai Van[2,*], Phien Vu Dinh[2], Khuyen Truong Manh[1], Cuong Dan Quoc[3]
[1]Faculty of Civil Engineering, Hanoi Architectural University.
anhlt@hau.edu.vn, khuyentm@hau.edu.vn
[2]Advanced Materials and Intelligent Systems for Infrastructure and High-Speed Rail (AMIS-HSR) research group, University of Transport Technology, Hanoi, Vietnam.
chienmv@utt.edu.vn, phienvd@utt.edu.vn
[3]Faculty of Information Technology, Hanoi Architectural University.
cuongdq@hau.edu.vn

Article info
Type of article:
Original research paper

DOI:
https://doi.org/10.58845/jstt.utt.2025.en.5.4.218-237

***Corresponding author:**
Email address:
chienmv@utt.edu.vn

Received: 29/09/2025
Received in Revised Form: 27/11/2025
Accepted: 15/12/2025

Abstract: Accurate classification of failure modes in reinforced concrete (RC) shear walls is essential for performance-based seismic design, yet current code-based criteria rely mainly on simple geometric indicators and cannot fully capture the nonlinear interaction among geometry, axial load, reinforcement, and boundary confinement. This study develops a mechanics-aware machine learning (ML) framework to classify four experimentally observed failure modes flexural (F), flexure shear (FS), shear (S), and sliding (SL) using both dimensional and non-dimensional feature spaces. The experimental data used in this study are analysed through two complementary representations: a dimensional dataset (CSDL1, 435 specimens) based on conventional geometric and material parameters, and a non-dimensional, mechanics-informed dataset (CSDL2, 569 specimens) expressed in terms of physically motivated ratios (A_b/A_g, l_w/t_w, $P/(f_c'A_g)$, ρ_{fy}/f_c'), both constructed from the same body of published experimental studies. Three representative tree-based algorithms—Decision Tree, Random Forest, and XGBoost were trained and evaluated using 70/30 train–test splits, 10-fold cross-validation, confusion matrices, and AUC–ROC metrics. All models achieved strong multi-class performance with average AUC values above 0.85. Random Forest provided the most stable generalisation across both feature representations, while XGBoost attained comparable accuracy. More importantly, the non-dimensional feature space enhanced physical interpretability: SHAP analysis consistently identified the boundary-to-gross area ratio (A_b/A_g) and wall slenderness (l_w/t_w) as the dominant predictors for all failure modes, followed by reinforcement and axial-load ratios. The ML-derived transition thresholds ($A_b/A_g \approx 0.08–0.12$, $l_w/t_w \approx 8–12$, $M/(Vl_w) \approx 0.4$, and $P/(f_c'A_g) \approx 0.1$) align well with conceptual limits in ACI 318 and Eurocode 8. The study therefore demonstrates that mechanics-informed, non-dimensional features not only

Journal of Science and Transport Technology
Journal homepage: https://jstt.vn/index.php/en

Abstract: (continued) sustain high predictive accuracy but also recover the underlying physics of wall behaviour, enabling design-oriented summary tables and a quick failure-mode classification checklist for practical seismic design and assessment.

Keywords: Reinforced concrete shear walls, failure mode classification, machine learning, dimensional analysis, non-dimensional features, XGBoost, Random Forest, SHAP, feature importance, seismic design.

1. Introduction

Reinforced concrete (RC) shear walls are fundamental lateral load resisting components in modern reinforced concrete structures, particularly in regions of high seismicity. Under combined axial compression and in plane lateral loading, these walls may fail through distinct mechanisms depending on their geometric proportions, reinforcement configuration, axial load level, and boundary confinement conditions [1],[2],[3]. Accurate prediction of failure mechanismsflexural (F), flexure–shear (FS), shear (S), and sliding (SL) is essential for performance-based seismic design, as these modes exhibit markedly different ductility, energy dissipation capacity, and post yield behavior [4].

Existing design standards such as ACI 318-19, Eurocode 8 (EN 1998-1:2023), and CSA A23.3-19 classify wall behavior primarily based on geometric indicators like aspect ratio (h_w/l_w) or empirical limits on shear-to-flexural strength ratios [5],[6],[7]. However, such simplified criteria fail to capture the complex, nonlinear, and multidimensional interactions among geometry, material properties, and load effects that govern wall behavior [8],[9]. Experimental investigations have consistently demonstrated that the transition between different failure modubu es is not governed by a single variable but by the combined influence of axial load ratio, reinforcement detailing, and boundary confinement [1],[3].

In recent years, machine learning (ML) has emerged as a powerful approach for predicting structural behavior, capable of learning nonlinear, high dimensional relationships from experimental data without relying on explicit constitutive models. Applications in structural engineering have included concrete strength prediction [10], structural damage detection [11], and seismic response modeling [12],[13],[14],[15]. For RC shear walls, several studies have developed ML-based models to predict shear strength [16], but failure mode classification a critical factor determining drift capacity and design detailing has received limited attention. Integrating both strength prediction and mode classification provides a comprehensive basis for understanding the seismic performance of RC walls.

A key limitation of existing ML approaches lies in their reliance on dimensional features (e.g., mm, kN, MPa), which are sensitive to unit systems, scale effects, and lack physical interpretability. In contrast, non-dimensional (dimensionless) parameters such as aspect ratio (a/d), reinforcement indices (ρ_l, ρ_t), and axial load ratio (P/f_cA_g) are widely recognized in structural mechanics for representing fundamental behavioral ratios that remain invariant to scale [17]. Such normalized variables can enhance the generalization and physical interpretability of ML models, particularly in problems governed by mechanical similitude.

Accordingly, this study aims to develop and compare machine learning models for predicting shear strength and classifying failure modes of RC shear walls using both dimensional and non-dimensional feature spaces. Two comprehensive experimental databases were compiled and harmonized: (i) CSDL1 (435 specimens) with dimensional parameters, and (ii) CSDL2 (569 specimens) with normalized mechanical ratios. Three representative ML algorithms Decision Tree, Random Forest, and XGBoost are employed to evaluate the influence of feature representation on model performance, generalization, and interpretability.

Beyond predictive capability, this research emphasizes model explainability through the SHAP (SHapley Additive Explanations) framework, enabling the identification of the most influential features and their physical significance. By linking statistical feature importance to mechanical principles, the study bridges data-driven prediction with structural interpretation, ensuring that ML models not only predict accurately but also remain consistent with the underlying physics of wall behavior.

The anticipated contributions of this study are threefold:

(1) Establishing a systematic comparison between dimensional and non-dimensional datasets for ML-based prediction of RC shear wall behavior;

(2) Developing a physics-informed interpretive framework that integrates SHAP-based feature analysis with structural mechanics concepts; and

(3) Providing insights to support data-driven calibration of design equations and seismic design guidelines.

2. Background and Theoretical Basis

2.1. RC Shear Wall Failure Modes and Mechanical Characteristics

When subjected to combined axial compression and in-plane lateral loading, reinforced concrete (RC) shear walls may fail through four principal mechanisms as shown in Fig. 1, including: flexural (F), flexure–shear (FS), shear (S), and sliding (SL). Each failure mode reflects a distinct internal stress redistribution and deformation pattern, and is recognised in major seismic design standards such as [5],[6],[7],[18]. These mechanisms are governed by the relative dominance of flexural, shear, or sliding actions, as well as the contribution of vertical and horizontal reinforcement to energy dissipation and ductility capacity [1],[3],[4].

(a) Flexural Failure (F)

Flexural failure typically occurs in slender walls (h_w/l_w > 3.0) where bending deformation dominates over shear distortion. The response is governed by flexural yielding of longitudinal reinforcement at the wall boundaries, accompanied by concrete crushing in the compression toe, forming a well-defined plastic hinge at the base [5], [6],[19].

Vertical reinforcement primarily resists the bending moment and controls vertical cracking, while horizontal reinforcement confines the boundary region and prevents bar buckling. The behavior is ductile, characterized by stable post-yield stiffness, large lateral drift capacity (δ > 2%), and high hysteretic energy dissipation [4]. This mode is regarded as the desired ductile mechanism in seismic design because it allows controlled plastic hinge formation before strength degradation.

(b) Flexure–Shear Failure (FS)

The flexure–shear mode represents a hybrid transition mechanism that occurs in moderately slender walls (1.5 < h_w/l_w < 3.0) where both flexural and shear deformations are significant. Initially, vertical flexural cracks form near the wall base, followed by the development of inclined diagonal cracks in the web once the principal tensile stress exceeds the concrete tensile strength.

This behavior reflects a gradual transition from flexure-dominated to shear-dominated response, accompanied by stiffness degradation

and mixed deformation patterns [5],[6],[19]. The interaction between flexural yielding and diagonal shear cracking results in moderate ductility (1% < δ < 2%), with energy dissipation reduced compared to pure flexural behavior. The horizontal reinforcement enhances shear transfer and limits crack widening, while vertical reinforcement maintains ductility and delays brittle diagonal failure [1],[20].

(c) Shear Failure (S)

Shear failure occurs predominantly in squat walls (h_w/l_w < 1.5) with high shear demand or insufficient horizontal web reinforcement. The failure mechanism is governed by diagonal tension cracking and diagonal compression strut crushing, which cause abrupt loss of strength and stiffness [5],[7].

When the shear stress $v = V/(b_w d)$ exceeds approximately $0.25\sqrt{f_c'}$ (in MPa), brittle failure may occur. The horizontal reinforcement provides the primary resistance against diagonal tension and prevents crack propagation, while the vertical reinforcement enhances confinement and anchorage at the wall boundaries. The overall behavior is brittle, characterized by low ductility (δ < 1%), sudden strength degradation, and small drift capacity [3],[4].

(d) Sliding Shear Failure (SL)

Sliding shear failure is governed by horizontal slip along a base interface or construction joint, often after extensive flexural cracking and yielding have degraded the shear transfer mechanisms. It is characterized by the formation of a dominant horizontal crack at or near the wall base, followed by relative displacement between upper and lower wall segments [5],[6], [19]. This mechanism is controlled by aggregate interlock, dowel action of vertical bars, and frictional resistance along the sliding plane. Vertical reinforcement improves dowel action and frictional resistance, while horizontal reinforcement provides clamping action and enhances shear resistance. Sliding failure is typically observed in walls with insufficient shear keys or weak construction joints, and exhibits abrupt strength loss and limited energy dissipation [1],[20].

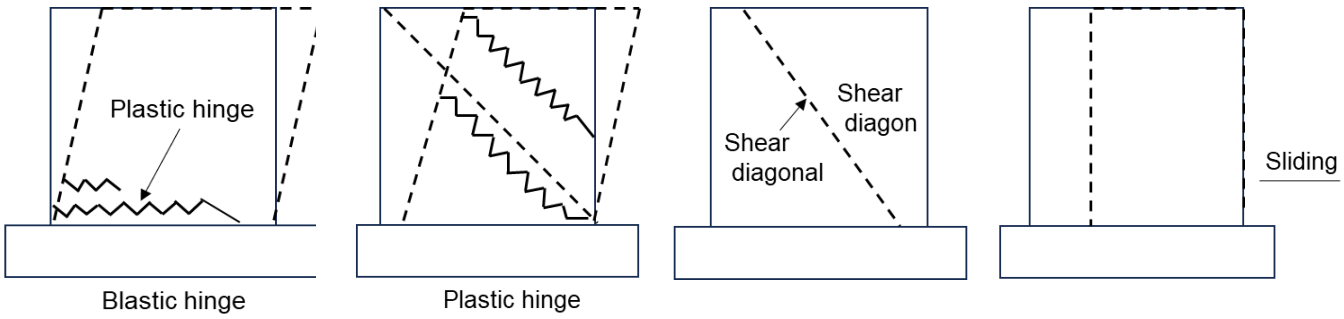

Fig. 1. Schematic illustrations of the four failure modes with typical crack patterns and deformed shapes

2.2. Physical Interpretation of Dimensional and Non-Dimensional Parameters

Experimental data for RC shear walls are typically recorded in dimensional form with physical units (e.g., kN for forces, MPa for stresses, mm for dimensions). While these measurements directly reflect laboratory observations, dimensional parameters are inherently scale-dependent and sensitive to unit systems, which limits their ability to represent the fundamental physics governing structural behaviour across different specimen sizes and configurations. Non-dimensional parameters, derived through normalisation by characteristic mechanical quantities, capture the essential physics while being invariant to unit systems and specimen scale. This transformation from dimensional to non-dimensional space is grounded in dimensional analysis principles [21] and has been standard practice in mechanics for over a century. For RC shear walls, appropriate

non-dimensional parameters arise naturally from equilibrium, compatibility, and constitutive relationships. The transformation can be expressed conceptually as:

Table 1. Non-dimensional parameters and their physical significance

No	Symbol	Physical Interpretation	Mechanical Significance
1	M/Vl_w	Ratio between the bending moment and the product of shear force and wall length.	Reflects the degree of interaction between flexural and shear actions, indicating the tendency of the wall to fail in flexure or shear.
2	l_w/t_w	Ratio between wall height and wall thickness.	Represents the geometric slenderness of the wall – slender walls tend to flexural behavior, while squat walls are shear-dominated.
3	$\rho_v f_{yv}/f_{ck}$	Ratio between the product of longitudinal reinforcement ratio and steel yield strength to concrete compressive strength.	Indicates the contribution of longitudinal reinforcement to the flexural capacity and the ability to resist combined flexure–shear behavior.
4	$\rho_h f_{yh}/f_{ck}$	Ratio between the product of horizontal web reinforcement ratio and steel yield strength to concrete compressive strength.	Characterizes the ability of horizontal reinforcement to restrain diagonal cracking and enhance shear resistance of the wall web.
5	$\rho_L f_{yL}/f_{ck}$	Ratio between the product of boundary longitudinal reinforcement ratio and steel yield strength to concrete compressive strength.	Represents the role of boundary elements in improving flexural confinement and delaying the onset of boundary crushing failure.
6	$P/f_{ck}A_g$	Ratio between axial load and nominal compressive capacity of the cross-section.	Reflects the influence of axial load on the interaction between shear and flexural responses, affecting failure mode transitions.
7	Shape of Section	Geometric shape of the wall cross-section (B: Barbell; R: Rectangular; E: Flanged).	Defines the sectional type, which governs the stress distribution, stiffness, and strength characteristics of the wall.
8	A_b/A_g	Ratio between boundary reinforcement area and gross cross-sectional area.	Quantifies the concentration of boundary reinforcement, closely related to the wall's shear strength and confinement capacity.

Dimensional data → Normalisation by characteristic mechanical quantities → Non-dimensional parameters.

Table 1 summarises the key non-dimensional parameters employed in this study, their mechanical interpretation, and their relationship to failure mode transitions.

By expressing all features in non-dimensional form, the models become physically meaningful, scale-independent, and directly aligned with dimensionless groups that appear naturally in theoretical formulations and code provisions. This physics-informed feature engineering is hypothesised to enhance both model generalisation and interpretability.

3. Experimental Database and Feature Engineering

3.1. Data Sources and Collection Methodology

The experimental data used in this study are drawn from a common pool of published RC shear

wall tests and are analysed using two complementary feature representations: a dimensional dataset (CSDL1) and a non-dimensional, mechanics-informed dataset (CSDL2):

CSDL1 (435 specimens): A dataset originally assembled by [22], [23], [24], [25], [26], [27, p. 31], [27], [28], [29], [30], [31], [32], covering tests published between 1970 and 2020 from peer-reviewed journals and conference proceedings. This database includes a wide range of wall geometries, reinforcement configurations, and loading protocols.

CSDL2 (569 specimens): An independently compiled dataset focusing on more recent experimental campaigns (1970-2020) [22], [23], [24], [25], [26], [27, p. 31], [27], [28], [29], [30], [31], [32], with enhanced representation of modern high-strength concrete walls and non-conventional reinforcement layouts.

Each specimen record includes: Geometric parameters: wall height (h_w), length (l_w), web thickness (t_w), flange dimensions (b_f, t_f), cross-sectional shape (rectangular, barbell, flanged); Material properties: concrete compressive strength (f'_c), vertical web reinforcement ratio (ρ_v) and yield strength (f_{yv}), horizontal web reinforcement ratio (ρ_h) and yield strength (f_{yh}), boundary element longitudinal reinforcement ratio (ρ_L) and yield strength (f_{yL}); Loading conditions: applied axial load (P), experimental shear strength (V_{exp}), applied moment (M). Observed failure mode: classified as F, FS, S, or SL based on experimental observations and reported cracking patterns.

3.2. Data Harmonisation and Quality Control

A critical challenge in assembling multi-source databases is ensuring consistency in failure mode classification, as different researchers may apply varying criteria or subjective judgements. To address this issue, the following harmonisation procedure was implemented:

Step 1 – Literature Review: Original test reports and publications were retrieved and reviewed to verify reported failure modes based on photographic evidence, crack pattern descriptions, and load-displacement responses.

Step 2 – Classification Criteria: Consistent classification rules were applied based on:

- Flexural (F): Yielding of boundary reinforcement, concrete crushing at compression toe, vertical cracks predominantly near wall edges
- Flexure-Shear (FS): Initial flexural cracking followed by diagonal shear cracks in web region, partial yielding of boundary reinforcement
- Shear (S): Diagonal tension or compression failure, extensive web cracking, limited boundary yielding
- Sliding (SL): Dominant horizontal crack at base, significant slip displacement along crack plane

Step 3 – Ambiguous Cases: For specimens where failure mode classification was uncertain or conflicting between sources, the following tie-breaking procedure was applied: (a) prioritise classifications from original investigators, (b) cross-reference with photographic evidence when available, (c) exclude specimens with insufficient documentation.

Step 4 – Data Cleaning: Specimens with missing critical parameters, obvious reporting errors, or inconsistent units were removed. A total of more than 100 specimens were excluded during this quality control phase.

3.3. Class Distribution and Dataset Characteristics

Both datasets exhibit significant class imbalance, reflecting the empirical reality that shear and flexural failures are more commonly observed in RC shear wall testing programmes than sliding failures. Table 2 summarises the class distribution for both databases.

The class imbalance presents challenges for ML model training, as algorithms may develop bias toward majority classes. To address this issue, stratified sampling procedures and class-weighted loss functions were employed during model training (detailed in Section 5).

The statistical distribution of the input

variables by failure mode, as illustrated in Fig. 2, and Table 3, 4 reveals significant differences between the dimensional and non-dimensional feature spaces in terms of their mechanical characteristics.

(1) Geometric Parameters

Table 2. Failure mode class distribution in CSDL1 and CSDL2 datasets

Failure Mode	CSDL1 (n=435 samples)	CSDL2 (n=569 samples)
Flexural (F)	108 (24.83%)	172 (39.54%)
Flexure-Shear (FS)	51 (11.72%)	99 (22.76%)
Shear (S)	252 (57.93%)	275 (63.22%)
Sliding (SL)	14 (3.22%)	23 (5.29%)

Table 3. Features of shear strength database for RC walls of CSDL1

Features	Mean	Standard deviation	Minimum	25%	50%	75%	Maximum
h_w (mm)	1349,08	983,35	145,00	600,00	1200,00	1750,00	4572,00
l_w (mm)	1299,35	780,48	420,00	700,00	1000,00	1720,00	3960,00
t_w(mm)	96,19	49,35	10,00	67,00	100,00	125,00	203,00
t_f (mm)	69,65	79,00	0,00	0,00	60,00	102,00	360,00
b_f (mm)	324,84	398,88	42,00	100,00	160,00	400,00	3045,00
f_{ck} (MPa)	37,34	20,72	13,70	23,50	32,80	43,40	130,80
ρ_v (%)	0,82	0,84	0,00	0,38	0,60	1,01	6,24
f_{yv} (MPa)	429,62	104,57	235,00	352,00	422,00	477,85	792,00
ρ_h (%)	0,70	0,48	0,00	0,33	0,57	0,92	3,67
f_{yh} (MPa)	430,37	108,83	235,00	350,00	405,00	504,00	806,00
ρ_L (%)	3,01	2,02	0,35	1,32	2,41	4,70	9,91
f_{yL} (MPa)	512,98	156,34	235,00	382,20	533,20	640,00	980,00
P (kN)	434,92	534,93	0,00	0,00	135,00	859,00	2364,00
V_{exp} (kN)	755,18	969,69	0,00	125,50	368,00	899,50	7060,00

Table 4. Features of shear strength database for RC walls of CSDL2

Features	Mean	Standard deviation	Minimum	25%	50%	75%	Maximum
M/Vl_w	1,22	0,69	0,25	0,66	1,00	1,76	4,10
l_w/t_w	14,92	8,30	4,35	10,00	13,33	18,68	57,00
ρ_v*f_{yv}/f_{ck}	0,09	0,07	0,00	0,04	0,07	0,11	0,49
ρ_h*f_{yh}/f_{ck}	0,08	0,06	0,00	0,04	0,07	0,11	0,33
ρ_L*f_{yL}/f_{ck}	0,34	0,33	0,00	0,14	0,25	0,42	2,65
$P/f_{ck}*A_g$	0,07	0,10	0,00	0,00	0,03	0,09	0,50
A_b/A_g	0,14	0,13	0,00	0,00	0,17	0,26	0,44

The results indicate that classes FS and SL exhibit higher median wall lengths (l_w) compared to other classes, while class S shows the widest interquartile range (IQR) and the largest absolute wall lengths. This reflects the tendency of shear–sliding failures to occur in taller and more slender walls. In contrast, class F has the lowest median l_w, representing flexural failures typical of short

walls with lower aspect ratios. After normalization by the wall thickness (l_w/t_w), the medians across classes become closer and the IQRs significantly narrower, indicating that the influence of absolute geometric scale has been removed. This highlights the role of slenderness as a key descriptor governing the failure mechanism. However, class S still maintains high variability and numerous outliers, suggesting that geometric dimensions alone cannot fully explain the differences in failure modes without considering the combined effects of axial load and reinforcement ratio.

(2) Axial Load Parameters

In the dimensional dataset, class F exhibits the highest median axial load (P), reflecting the higher compressive capacity of flexural-type walls. Class S presents the widest distribution range, consistent with the sensitivity of shear failures to variations in axial compression. After normalization into $P/(f_{ck}A_g)$, the data become more compact with smaller IQRs, but a greater number of outliers appear particularly in class F. This suggests that normalized axial load ratios vary notably among specimens, capturing the relative sensitivity of flexural mechanisms to axial load intensity compared with material strength.

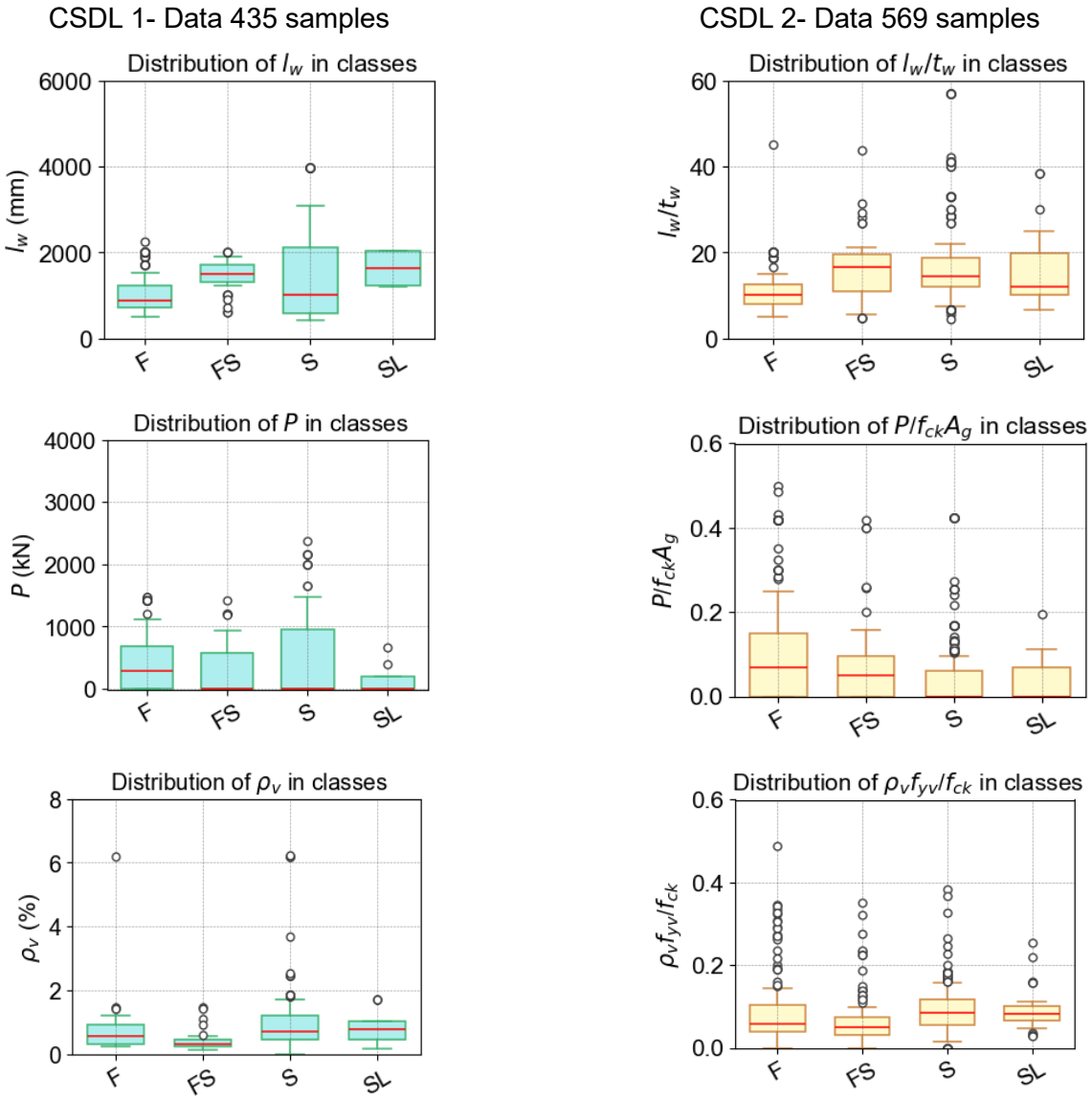

Fig. 2. Grap the box plot of CSDL 1 and CSDL 2

(3) Reinforcement Parameters

For vertical reinforcement in the wall web (ρ_v), the median values are generally similar across failure classes, although some samples in

classes S and F exhibit higher values, reflecting local reinforcement enhancement to improve bending and shear resistance. When normalized as $\rho_v f_{yv}/f_{ck}$, class medians converge, but the number of outliers increases significantly, indicating the combined influence of material strength and relative reinforcement levels.

Regarding horizontal reinforcement (ρ_h), all classes show comparable medians, but class S has a wider IQR and more outliers, corresponding to its role in resisting diagonal cracking and enhancing shear strength. In the non-dimensional space ($\rho_h f_{yh}/f_{ck}$), the IQRs of all classes increase and more outliers appear, reflecting the diversity in the relationship between stirrup strength and concrete compressive strength. For boundary longitudinal reinforcement (ρ_L), the dimensional dataset shows higher median values for classes FS and SL compared to classes F and S, indicating strengthened boundary regions in walls subjected to flexure–shear and shear–sliding actions. However, in the normalized dataset ($\rho_L f_{yL}/f_{ck}$), the medians become closer, IQRs narrow, and outlier counts rise, demonstrating that relative reinforcement and material strength effects become more pronounced once geometric scaling is removed.

Normalization effectively eliminates the influence of absolute geometric scale and highlights the relative interplay among geometry, axial load, and material–reinforcement properties. The non-dimensional variables show convergence in median values but an increase in outlier frequency, reflecting the inherent variability in the interaction between material strength and reinforcement ratios. Overall, the distinctions among failure modes are not governed solely by geometry or load intensity, but are strongly influenced by the combined interaction of geometry materialreinforcement characteristics, which becomes more evident in the non-dimensional data space.

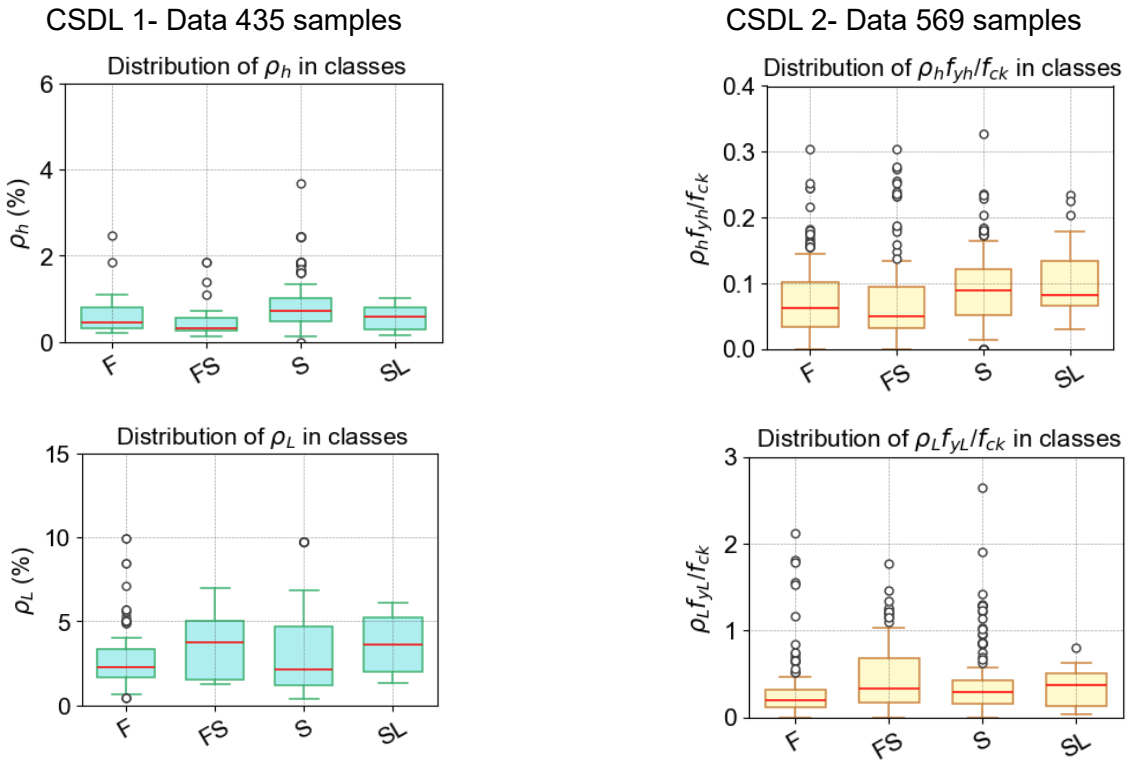

Fig. 2. (continued)

4. Machine Learning Methodology

In this study, three representative machine learning models were selected to evaluate and compare their capability in classifying failure modes of reinforced concrete (RC) shear walls: Decision Tree (DT), Random Forest (RF), and

Extreme Gradient Boosting (XGBoost).The Decision Tree and Random Forest algorithms are widely recognised for their interpretability and have been extensively applied in structural engineering to predict material strength, identify failure modes, and model nonlinear structural behaviour [10], [12]. In contrast, XGBoost represents a more advanced gradient boosting approach capable of capturing highly nonlinear and interactive relationships among geometric, material, and load-related parameters, while maintaining high prediction accuracy and stability in multi-class classification problems [33].

These three models were selected to achieve a balance between interpretability and predictive performance, enabling both mechanics-based feature interpretation through SHAP analysis and robust evaluation of model accuracy and generalisation in RC shear wall failure mode classification.

4.1. Decision Tree (DT)

The Decision Tree is a non-parametric supervised learning algorithm that recursively divides the dataset into non-overlapping subregions through hierarchical binary decisions [34]. Each internal node represents a split based on a specific input variable, while each terminal node (leaf) corresponds to a predicted output class. Tree induction involves two stages: (1) Tree building, where data are partitioned using impurity metrics such as the Gini Index or information gain, and (2). Tree pruning, where redundant branches are removed to prevent overfitting [35]. In this study, cost–complexity pruning was applied, and the pruning parameter was optimized via 10-fold cross-validation to achieve the best generalisation performance.

4.2. Random Forest (RF)

The Random Forest algorithm, proposed by [36], is an ensemble learning technique that constructs multiple decision trees using bootstrap samples and random feature subsets [37]. Each tree independently contributes a classification result, and the final output is determined by majority voting. This combination reduces overfitting, enhances robustness, and allows the model to capture complex nonlinear relationships. Moreover, Random Forest provides feature importance estimates, derived from either impurity reduction (Gini importance) or permutation-based measures, enabling physical interpretation of the influence of each variable on the predicted failure mode.

4.3. Extreme Gradient Boosting (XGBoost)

The XGBoost algorithm [33] is a powerful extension of the gradient boosting framework that builds an ensemble of weak learners (typically shallow trees) in a sequential manner. At each iteration, a new tree is trained to minimize the residual errors (negative gradients) of the previous model, thus improving classification accuracy. XGBoost incorporates regularization terms (L_1 and L_2) to control model complexity and employs parallelized computation for high efficiency. Compared with Random Forest, XGBoost focuses on sequential gradient optimization rather than independent bagging, making it particularly effective for modeling nonlinear and coupled structural behaviors, such as interactions among axial load, geometry, and reinforcement ratios in RC shear walls.

5. Identification of Failure Modes Using Machine Learning Models

The machine learning (ML) algorithms described in the previous section were employed to classify the failure modes of reinforced concrete (RC) shear walls using two complementary feature representations derived from the same experimental literature. The models were implemented using the open-source Python library Scikit-learn [38].

For each feature representation, 70% of the specimens were randomly selected for model training, while the remaining 30% were reserved as an independent test set for final performance evaluation. Within the training set, 10-fold cross-validation combined with Gaussian-process-based Bayesian optimisation was used exclusively for

hyperparameter tuning, whereas the test set did not participate in either tuning or model selection.

The classification performance of the ML models was evaluated using confusion matrices, as illustrated in Figs. 3 and 4 and summarised in Table 5. Each element $C_{ij}(i,j = 1,2,3,4)$ represents the number of specimens with the actual failure mode ipredicted as mode j. The diagonal elements (C_{ii}) indicate correctly classified cases, while the off-diagonal elements correspond to misclassifications. Model performance was quantified using Accuracy, Precision, Recall, and F1-score.

Accuracy measures the overall proportion of correct predictions across all classes. Precision represents the proportion of samples predicted to belong to a given class that truly belong to that class. Recall denotes the proportion of actual samples in a given class that are correctly identified by the model.

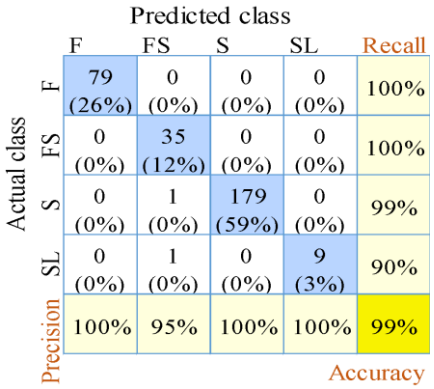

Average Accuracy (10-Fold CV on training set): 0.8783

a) Decision Tree – training set

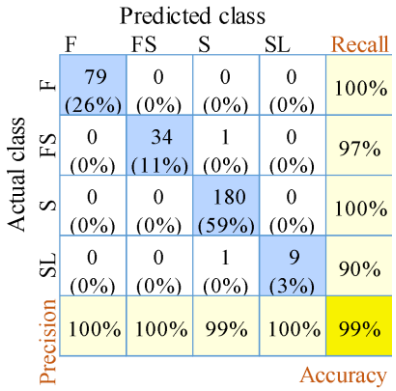

Average Accuracy (10-Fold CV on training set): 0.8946

b) Random Forest - training

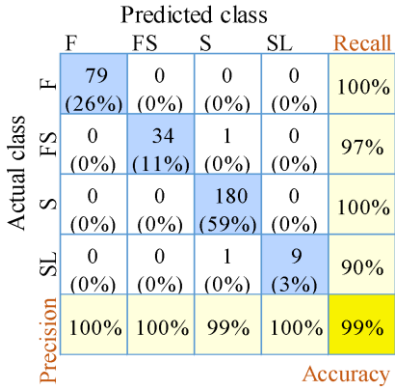

Average Accuracy (10-Fold CV on training set): 0.9080

c) XGBoost - training

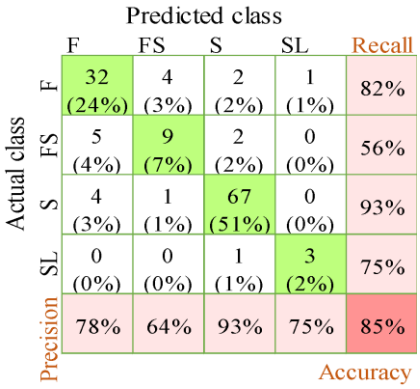

d) Decision Tree – testing set

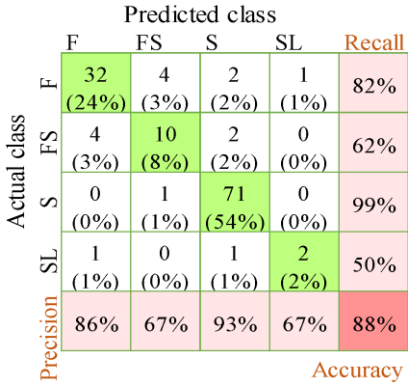

e) Random Forest – testing set

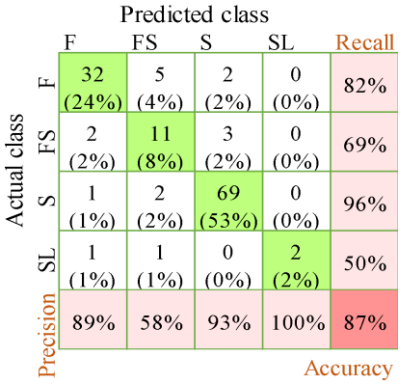

f) XGBoost – testing set

Fig. 3. Confusion matrix of classification models of various machine learning techniques using the training set and testing set for CSDL1: a) Decision Tree, b) Random Forest, g) XGBoost

In addition, to provide a more comprehensive evaluation of classification performance, the Area Under the ROC Curve (AUC) was calculated for each failure mode, as shown in Fig. 5. Higher AUC values indicate better class separability and greater model robustness across both datasets.

The confusion matrices for the two datasets – CSDL1 (dimensional) and CSDL2 (non-dimensional) – reveal distinct differences in model generalization and stability. For CSDL1, all three models achieved high accuracy, with Random Forest (RF) performing best (Accuracy = 0.88 on the testing set) owing to its strong capability in capturing nonlinear interactions among geometric, loading, and reinforcement parameters. XGBoost (XGB) ranked second (Accuracy = 0.87), exhibiting consistent predictions across classes, particularly for Flexural (F) and Shear (S) failures where Recall

was nearly 100%. Conversely, Decision Tree (DT), though highly interpretable, showed mild overfitting, reducing its accuracy for transitional classes such as FS and SL.

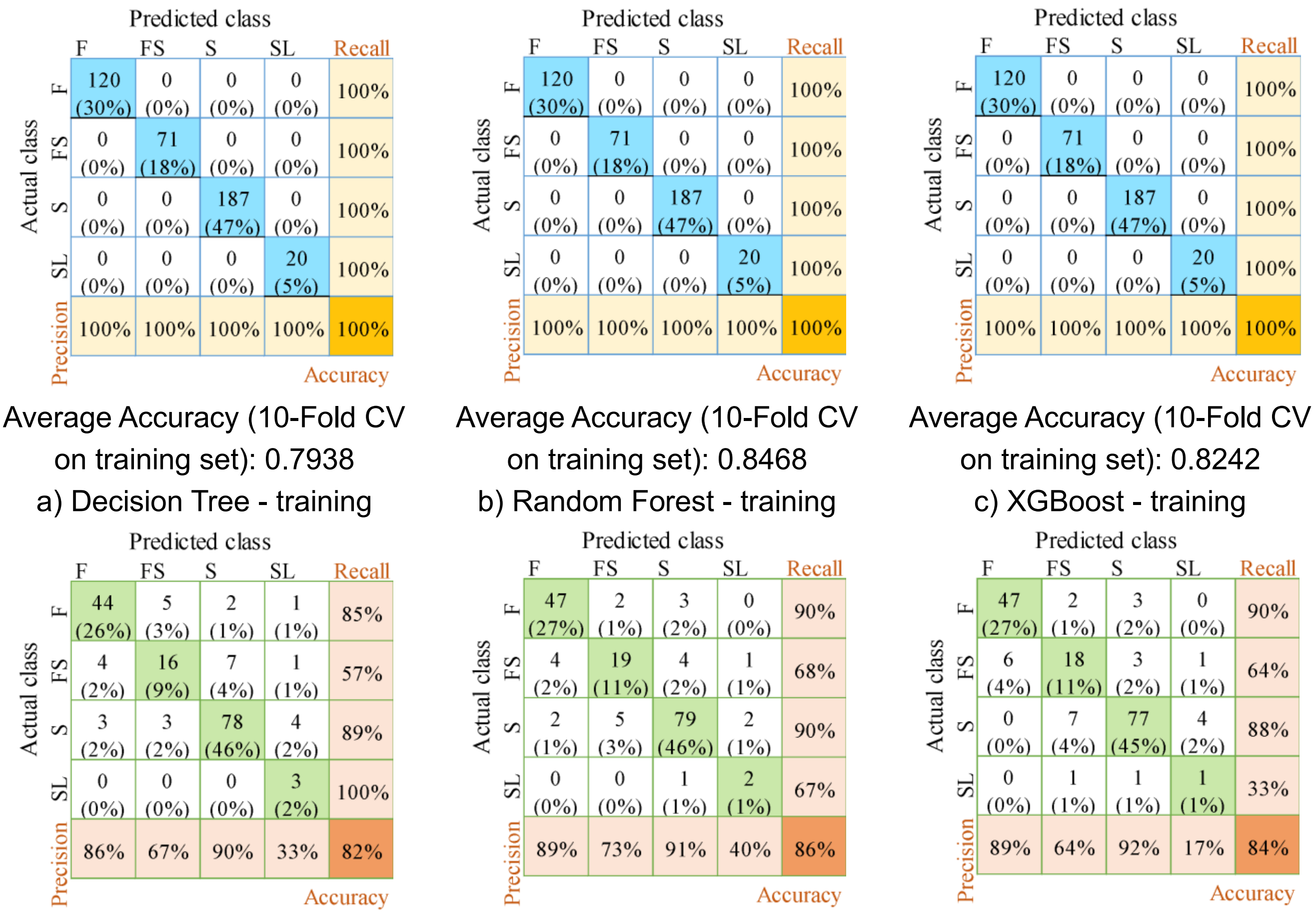

a) Decision Tree - training; b) Random Forest - training; c) XGBoost - training

d) Decision Tree – testing set; e) Random Forest – testing set; f) XGBoost – testing set

Fig. 4. Confusion matrix of classification models of various machine learning techniques using the training set and testing set for CSDL2: a) Decision Tree, b) Random Forest, g) XGBoost

For CSDL2 (non-dimensional), the overall model stability improved as normalization eliminated the effects of units and scale. Random Forest remained the most stable model (Accuracy = 0.86), maintaining consistent classification across failure types and minimal deviation between training and testing sets. XGBoost also performed well (Accuracy = 0.84) but showed greater Recall variation in the SL class, reflecting sensitivity to class imbalance. Decision Tree, on the other hand, showed lower accuracy and reduced robustness due to its reliance on sample distribution.

Overall, Random Forest demonstrated superior generalization and robustness across both datasets, while XGBoost achieved the highest accuracy on CSDL1 and maintained competitive performance on CSDL2. However, a closer look at the Precision–Recall results indicates that the discrepancies between intermediate classes (FS, SL) were more pronounced in the non-dimensional dataset than in the dimensional one. This phenomenon can be attributed to the loss of absolute physical scaling (moment, shear, axial load, wall height, and thickness) during normalization, which blurs the mechanical boundaries between flexure–shear and sliding mechanisms. As a result, when all features are represented as relative ratios, the models' ability to distinguish transitional behaviors diminishes, leading to greater variability in Precision and Recall.

In summary, the non-dimensional data representation enhances statistical consistency and generalization capability but simultaneously

reduces the mechanical separability of overlapping failure mechanisms, particularly between FS and SL modes.

The AUC–ROC results demonstrate that all three models—Decision Tree, Random Forest, and XGBoost achieved strong classification performance, with average AUC values exceeding 0.85, indicating reliable discrimination of RC shear wall failure modes. For CSDL1 (dimensional data), both Random Forest and XGBoost exhibited superior separation capability with AUC values ranging from 0.87 to 0.99, particularly stable for S and SL classes, while Decision Tree performed less consistently, especially for the transitional FS class (AUC = 0.77). This suggests that ensemble and boosting methods can capture nonlinear relationships among geometric, loading, and reinforcement parameters more effectively than single-tree models. In CSDL2 (non-dimensional data), the ensemble models showed slightly improved stability and generalization. Random Forest maintained the highest overall AUC (0.91–0.98), while XGBoost remained competitive (AUC ≈ 0.90–0.97) with minor variation in the FS class due to class imbalance. Although normalization improved statistical robustness, it slightly blurred the physical distinctiveness of variables, making the mechanical boundaries between FS and SL less pronounced. Overall, Random Forest proved to be the most stable and consistent model across both datasets, while XGBoost delivered the highest discrimination accuracy among the failure modes.

Table 5. Summary table of prediction results on the test sets of the two databases

Testing - CSDL1 (435 samples)						
No	**Models**	**Class**	**Precision**	**Recall**	**F_1 - score**	**Accuracy**
1	**DT**	F	78%	82%	80%	85%
		FS	64%	56%	60%	
		S	93%	93%	93%	
		SL	75%	75%	75%	
2	**RF**	F	86%	82%	84%	88%
		FS	67%	62%	65%	
		S	93%	99%	96%	
		SL	67%	50%	57%	
3	**XGB**	F	89%	82%	85%	87%
		FS	58%	69%	63%	
		S	93%	96%	95%	
		SL	100%	50%	67%	
Testing - CSDL2 (569 samples)						
No	**Models**	**Class**	**Precision**	**Recall**	**F_1 - score**	**Accuracy**
1	**DT**	F	86%	85%	85%	82%
		FS	67%	57%	62%	
		S	90%	89%	89%	
		SL	33%	100%	50%	
2	**RF**	F	89%	90%	90%	86%
		FS	73%	68%	70%	
		S	91%	90%	90%	
		SL	40%	67%	50%	
3	**XGB**	F	89%	90%	90%	84%
		FS	64%	64%	64%	
		S	92%	88%	90%	
		SL	17%	33%	22%	

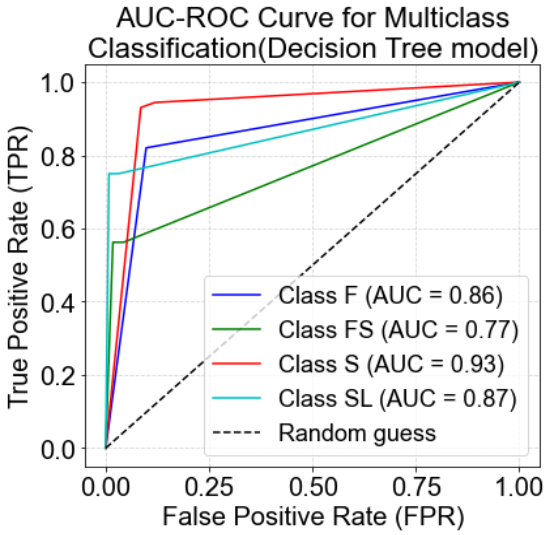

a) Decision Tree - CSDL1

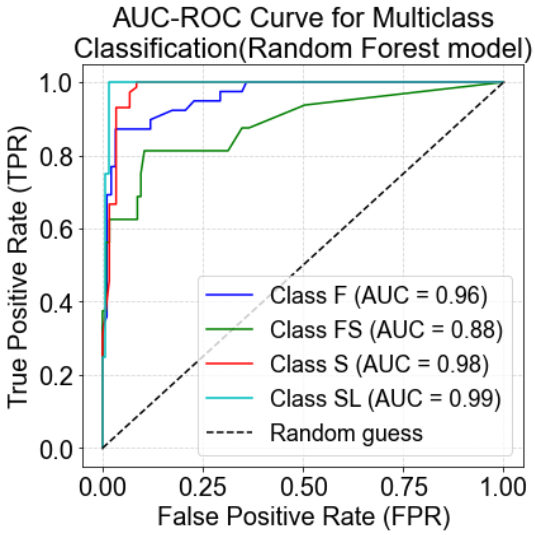

b) Random Forest - CSDL1

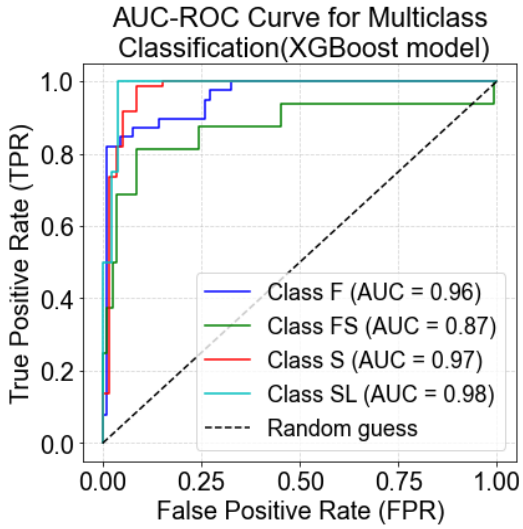

c) XGBoost - CSDL1

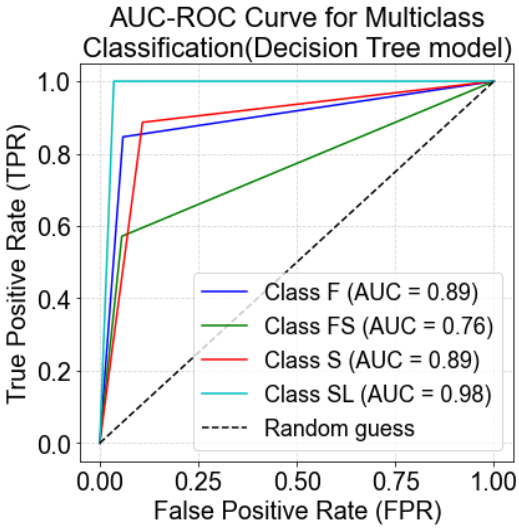

d) Decision Tree – CSDL2

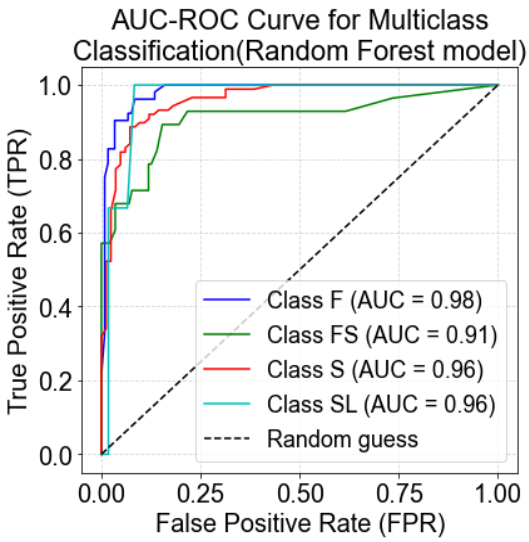

e) Random Forest – CSDL2

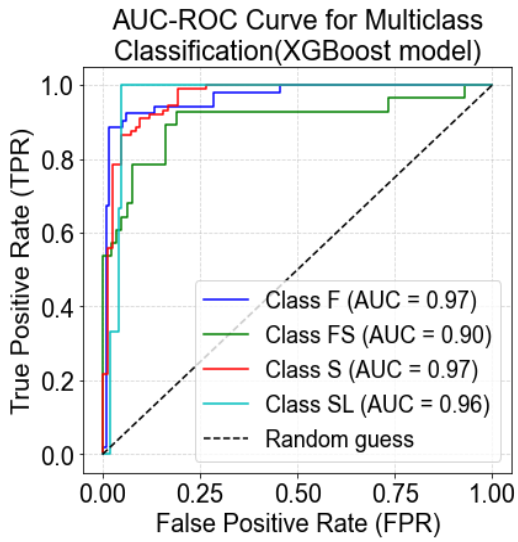

f) XGBoost - CSDL2

Fig. 5. Evaluation of Decision Tree, Random Forest, and XGBoost models based on AUC–ROC metrics for (CSDL1) and (CSDL2) datasets

6. SHAP-Based Feature Interpretation and Consistency with Structural Mechanics

The SHAP-based feature importance analysis provides valuable insights into how each geometric, material, and reinforcement parameter contributes to predicting the failure modes of RC shear walls. When these results are compared with the underlying physical mechanisms, it becomes evident that the machine-learning models correctly identify the dominant structural factors governing each failure mode. The results of the analysis are shown in Figs. 6 and 7 for the two datasets CSDL1 and CSDL2.

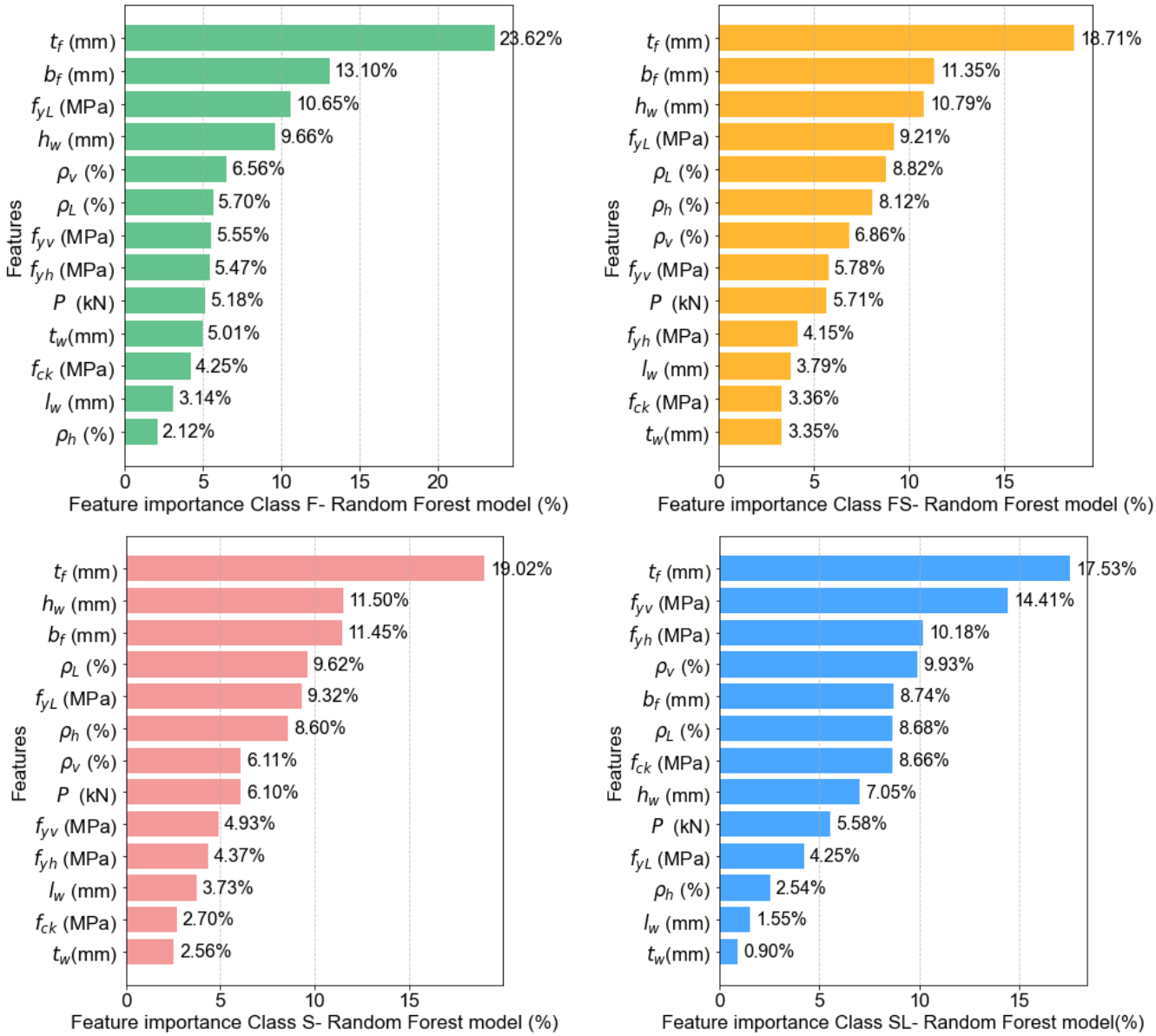

Fig. 6. The percentage importance of each feature for classification model – Random forest of CSDL1

The results demonstrate that transforming the dataset into a non-dimensional feature space is essential for accurately capturing the mechanics of failure in reinforced concrete shear walls. Unlike dimensional features which introduce scale dependence and lead the machine-learning model to overemphasize absolute geometric quantities the non-dimensional representation enables the Random Forest classifier to recover the correct physical behavior across all four primary failure modes: flexural (F), flexural–shear (FS), shear (S), and sliding-shear (SL). Notably, two parameters consistently emerge as the dominant predictors in every failure mode: the boundary area ratio

A_b/A_g and the wall slenderness ratio l_w/t_w. This finding aligns closely with structural mechanics: boundary elements dictate flexural capacity and ductility, while wall slenderness governs the transition between flexural-dominated and shear-dominated responses. Reinforcement stress ratios such as $\rho_v f_{yv}/f_c'$ and $\rho_h f_{yh}/f_c'$ play secondary but meaningful roles in controlling cracking and increasing ductility.

A direct comparison with [12] highlights a key methodological improvement. In their study, boundary properties were encoded using a discrete section-type variable (R/F/B), which does not quantify the actual extent of boundary elements. Consequently, the importance of tecontinuous boundary ratio A_b/A_g with broad variability across specimens, enabling the ML model to correctly capture the link between boundary confinement, flexural capacity, and the transition from flexural to shear or sliding failures. As a result, A_b/A_g becomes the most influential variable in all failure modes (30–40%), consistent with the governing role of boundary elements in [5], [6].

These observations confirm that the non-dimensional dataset not only eliminates scale artifacts but also highlights the intrinsic physical relationships governing behavior: walls with strong boundary elements and large slenderness ratios tend to fail in flexure (F); walls with moderate boundaries and slenderness undergo flexural–shear (FS); squat walls with limited boundary reinforcement fail in shear (S); and when both boundary capacity and slenderness are low, sliding-shear (SL) becomes likely due to large base slip and frictional mechanisms. The transition thresholds identified by the ML modelsuch as $A_b/A_g > 0.12$, $l_w/t_w > 12$, or $P/(f_c' A_g) < 0.1$ align well with codified detailing limits in ACI 318 and Eurocode 8 as well as experimental observations.

Based on these findings, the study proposes design-oriented summary Table 6 and a quick classification checklist to assist engineers in predicting failure modes prior to nonlinear analysis. These tables consolidate the mechanical signatures of each failure mode, provide physical interpretations, and recommend specific detailing measures such as enhancing confinement for flexural failures, adding stirrups or diagonal reinforcement for flexural–shear behavior, increasing horizontal reinforcement for shear failures, and improving base friction or adding anchors for sliding-shear cases. These recommendations provide a foundation for developing machine-learning-informed design guidelines that may be incorporated into future structural standards in Vietnam.

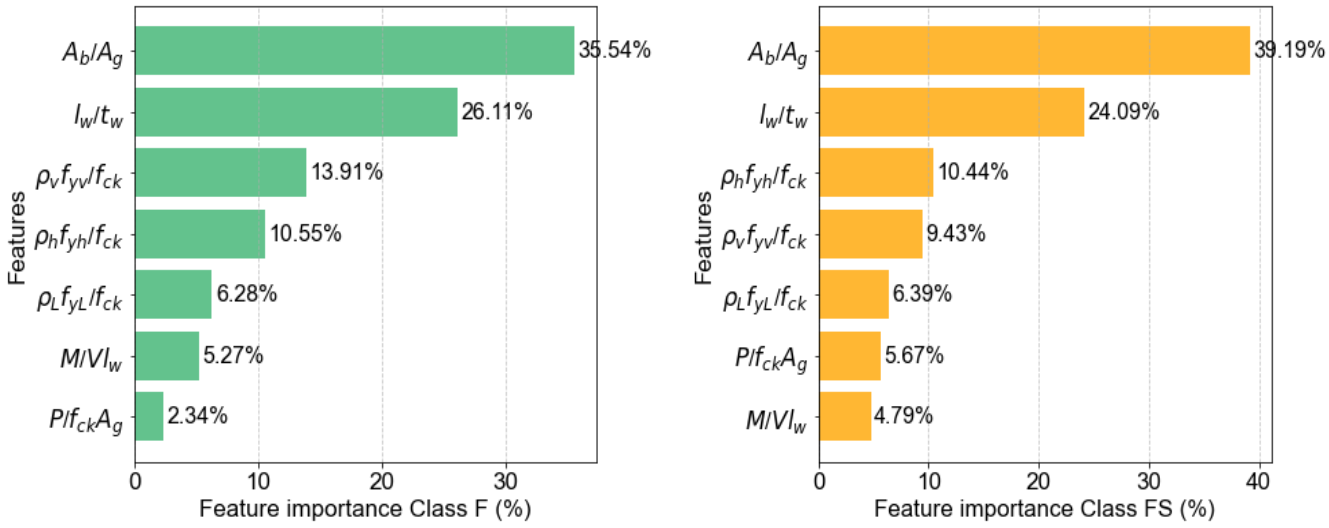

Fig. 7. The percentage importance of each feature for classification model – Random forest of CSDL2

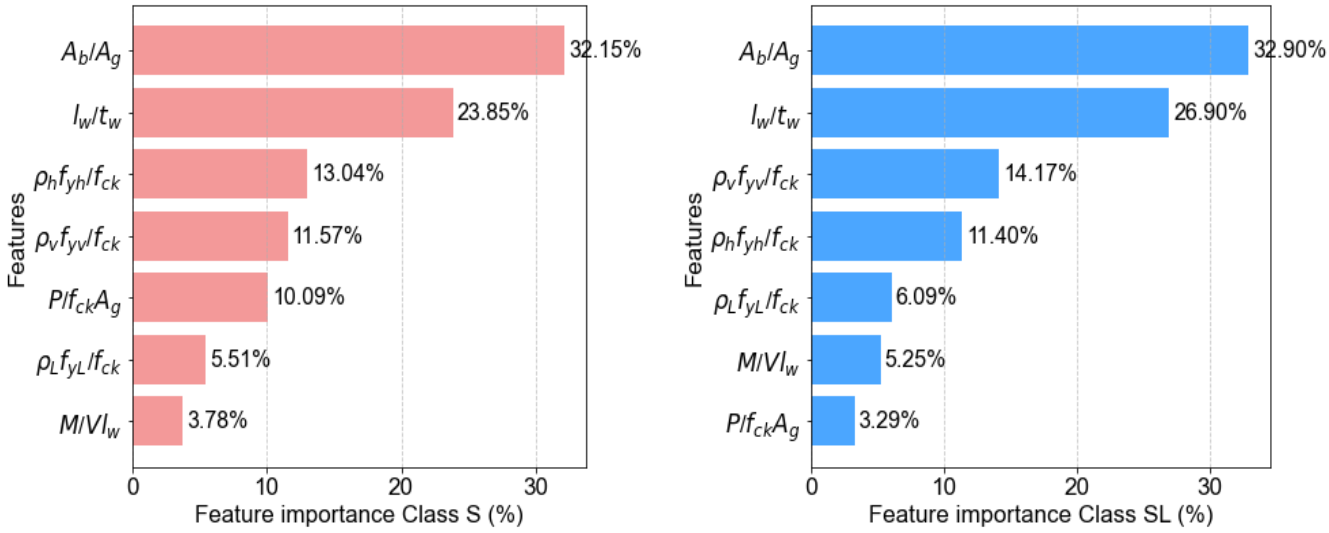

Fig. 7. (continued)

Table 6. ML thresholds, code limits, and recommended values

Variable	Threshold from ML	Code Limit (ACI/EC8)	Recommended Threshold
(A_b/A_g)	0.08–0.12	0.08–0.10 (ACI boundary element requirement)	0.08–0.12
(l_w/t_w)	8–12	≈ 10–12 (slender wall criterion, EC8)	8–12
$(M/(V\,l_w))$	0.3–0.4	≈ 0.4 (flexure–shear transition in nonlinear EC8)	0.4
$(P/(f'_c A_g))$	0.05–0.1	0.1 (typical axial load ratio, ACI)	0.1

7. Conclusion

This paper presented a mechanics-aware machine learning framework for classifying failure modes of reinforced concrete shear walls using both dimensional and non-dimensional feature spaces. A harmonised database was assembled from two sources and carefully checked for consistency in failure-mode labelling and parameter definitions. Three tree-based classifiers Decision Tree, Random Forest, and XGBoost were trained and validated through stratified train, test splits, k-fold cross-validation, confusion matrices, and AUC–ROC metrics. All models delivered strong performance, with average AUC values above 0.85, confirming that data-driven methods can reliably discriminate among flexural, flexure shear, shear, and sliding failures when provided with sufficiently rich experimental data. Random Forest exhibited the most stable generalisation across both datasets, whereas XGBoost achieved competitive accuracy, particularly for the dimensional feature set.

The comparison between dimensional (CSDL1) and non-dimensional (CSDL2) feature spaces highlights a crucial distinction. While dimensional variables allow slightly higher accuracy in some classes, they tend to bias the models toward absolute geometric scales and obscure the underlying mechanics. In contrast, the non-dimensional representation yields comparable accuracy but significantly improves physical interpretability. SHAP-based feature analysis consistently identifies the boundary-to-gross area ratio A_b/A_g and wall slenderness l_w/t_was the dominant predictors for all failure modes, supported by reinforcement and axial-load ratios. These findings are fully consistent with experimental observations and with the role of

boundary elements and aspect ratio emphasised in ACI 318 and Eurocode 8.

By analysing SHAP value transitions, the study proposes quantitative thresholds $A_b/A_g \approx 0.08 - 0.12$, $l_w/t_w \approx 8 - 12$, $M/(Vl_w) \approx 0.4$, and $P/(f'_c A_g) \approx 0.1$ that delineate the transition from flexural to flexure–shear, shear, and sliding-shear behaviour. These limits are consistent with code provisions and previous research yet are obtained independently from the data, providing a mechanics-informed validation of existing design criteria. The results are summarised in design-oriented tables and a quick classification checklist that link predicted failure modes to detailing recommendations, offering a practical tool for preliminary seismic assessment and design.

Despite these promising outcomes, several limitations remain. Class imbalance, particularly for sliding failure, may still influence the robustness of the models; future work should explore resampling strategies and larger experimental datasets. Moreover, the present models are developed for monotonic or quasi-static cyclic tests; extension to realistic earthquake loading histories and three-dimensional wall systems is a natural next step. Nonetheless, the study demonstrates the potential of mechanics-informed ML to bridge experimental databases, code provisions, and engineering judgement, and provides a foundation for future data-driven calibration of seismic design guidelines, including prospective updates to Vietnamese standards.

References

[1] T. Paulay, M.J.N. Priestley. (1992). Seismic Design of Reinforced Concrete and Masonry Buildings. *John Wiley & Sons, New York, NY*. DOI:10.1002/9780470172841

[2] I. Lefas, M.D. Kotsovos, N.N. Ambraseys. (1990). Behavior of Reinforced Concrete Walls Under Cyclic Loading. *Imperial College London, UK*.

[3] L.M. Massone, J.W. Wallace. (2004). Load-deformation responses of slender reinforced concrete walls. *ACI Structural Journal*, 101(1), 103–113. https://doi.org/10.14359/13003

[4] J.W. Wallace. (2012). Behavior, design, and modeling of structural walls and coupling beams – Lessons from recent laboratory tests and earthquakes. *International Journal of Concrete Structures and Materials*, 6(1), 3–18. https://doi.org/10.1007/s40069-012-0001-4

[5] American Concrete Institute (ACI). (2019). ACI 318-19: Building Code Requirements for Structural Concrete and Commentary.

[6] European Committee for Standardization (CEN). (2023). EN 1998-1:2023 – Eurocode 8: Design of structures for earthquake resistance – Part 1: General rules, seismic actions, and rules for buildings.

[7] Canadian Standards Association (CSA). (2019). CSA A23.3-19: Design of Concrete Structures.

[8] A. Deifalla, M.S. Khalil, A. Abdelrahman. (2015). Simplified model for the torsional strength of concrete beams with GFRP stirrups. *Journal of Composites for Construction*, 19(1), 04014032. https://doi.org/10.1061/(ASCE)CC.1943-5614.0000498

[9] H. Naderpour, M. Sharei, P. Fakharian, M.A. Heravi. (2022). Shear strength prediction of reinforced concrete shear wall using ANN, GMDH-NN and GEP. Journal of Soft Computing in Civil Engineering, 6(1), 66-87. https://doi.org/10.22115/SCCE.2022.283486.1308

[10] P.G. Asteris, A.D. Skentou, A. Bardhan, P. Samui, K. Pilakoutas. (2021). Predicting Concrete Compressive Strength Using Hybrid Ensembling of Surrogate Machine Learning Models. *Cement and Concrete Research*, 145, 106449.https://doi.org/10.1016/j.cemconres.2021.106449

[11] O. Abdeljaber, O. Avci, S. Kiranyaz, M. Gabbouj, D.J. Inman. (2017). Real-time vibration-based structural damage detection using one-dimensional convolutional neural

networks. *Journal of Sound and Vibration,* 388 154–170. https://doi.org/10.1016/j.jsv.2016.10.043

[12] S. Mangalathu, S.-H. Hwang, J.-S. Jeon. (2020). Failure mode and effects analysis of RC members based on machine-learning-based SHapley Additive exPlanations (SHAP) approach. *Engineering Structures,* 219, 110927. https://doi.org/10.1016/j.engstruct.2020.110927

[13] K. Le Nguyen, H.T. Trinh, S. Banihashemi, T.M. Pham. (2024). Machine learning approaches for lateral strength estimation in squat shear walls: A comparative study and practical implications. *Expert Systems with Applications,* 239, 122458. https://doi.org/10.1016/j.eswa.2023.122458

[14] K. Le Nguyen, H.T. Trinh, T.M. Pham. (2024). Prediction of punching shear strength in flat slabs: Ensemble learning models and practical implementation. *Neural Computing and Applications*, 36, 4207–4228. https://doi.org/10.1007/s00521-023-09296-0

[15] K. Le Nguyen. (2022). Application of XGBoost Model for Predicting the Dynamic Response of High-Speed Railway Bridges. *CIGOS 2021, Emerging Technologies and Applications for Green Infrastructure - Proceedings of the 6th International Conference on Geotechnics, Civil Engineering and Structures, pp. 1765–1773. Springer*. https://doi.org/10.1007/978-981-16-7160-9_178

[16] P. Parsa, H. Naderpour. (2021). Shear strength estimation of reinforced concrete walls using support vector regression improved by Teaching-learning-based optimization, Particle Swarm optimization, and Harris Hawks Optimization algorithm. *Journal of Building Engineering*, 44, 102593. https://doi.org/10.1016/j.jobe.2021.102593

[17] G.M. Calvi, M.J.N. Priestley, M.J. Kowalsky, G.H. Powell. (2008). Displacement-based seismic design of structures. *Earthquake Spectra*, 24(2), 555–571. https://doi.org/10.1193/1.2932170

[18] ACI-ASCE Committee 426. (1973). The Shear Strength of Reinforced Concrete Members. *Journal of the Structural Division*, 99(6), 1091–1187. https://doi.org/10.1061/JSDEAG.0003532

[19] American Society of Civil Engineers (ASCE). (2023). ASCE 41-23: Seismic Evaluation and Retrofit of Existing Buildings. Reston, VA.

[20] S. Xie, H. Lin, Y. Chen, R. Yao, Z. Sun, X. Zhou. (2025). Hybrid machine learning models to predict the shear strength of discontinuities with different joint wall compressive strength. *Nondestructive Testing and Evaluation,* 40(6), 2439–2459. https://doi.org/10.1080/10589759.2024.2381083

[21] E. Buckingham. (1914). On Physically Similar Systems; Illustrations of the Use of Dimensional Equations. *Physical Review*, 4(4), 345–376. https://doi.org/10.1103/PhysRev.4.345

[22] L.M. Massone, F. Melo. (2018). General solution for shear strength estimate of RC elements based on panel response. *Engineering Structures*, 172, 239–252. https://doi.org/10.1016/j.engstruct.2018.06.038

[23] C.-L. Ning, B. Li. (2017). Probabilistic development of shear strength model for reinforced concrete squat walls. *Earthquake Engineering & Structural Dynamics*, 46(6), 877–897. https://doi.org/10.1002/eqe.2834

[24] S. Sato, Y. Ogata, S. Yoshizaki, K. Kanata, T. Yamaguchi, T. Nakayama, Y. Inada, J. Kadoriku. (1989). Behavior of Shear Wall Using Various Yield Strength of Rebar, Part 1: An Experimental Study. *Proceedings of the Tenth International Conference on Structural Mechanics in Reactor Technology (SMiRT 10), H09/01, Anaheim, CA, USA.*

[25] J.-W. Baek, H.-G. Park, H.-M. Shin, S.-J.

Yim. (2017). Cyclic Loading Test for Reinforced Concrete Walls (Aspect Ratio 2.0) with Grade 550 MPa (80 ksi) Shear Reinforcing Bars. *ACI Structural Journal*, 114(3), 673–686. DOI: 10.14359/51689437

[26] S. Teng, J. Chandra. (2016). Cyclic Shear Behavior of High-Strength Concrete Structural Walls. *ACI Structural Journal*, 113(6), 1335–1345. DOI: 10.14359/51689158

[27] C.E. Ospina, G. Birkle, W. Widianto, et al. (2019). ACI 445/fib WG 2.2.3 Punching Shear Test Database 1. *DataCenterHub*.

[28] R. Illiya, V.V. Bertero. (1980). Effects of amount and arrangement of wall-panel reinforcement on hysteretic behavior of reinforced concrete walls (Report No. UCB/EERC-80/04). *Earthquake Engineering Research Center, University of California, Berkeley, CA.*

[29] J.M. Vallenas, V.V. Bertero, E.P. Popov. (1979). Hysteretic Behaviour of Reinforced Concrete Structural Walls. (Report No. UCB/EERC-79/20). *Earthquake Engineering Research Center, University of California, Berkeley, CA.*

[30] M. Hirosawa. (1975). Past experimental results on reinforced concrete shear walls and analysis on them (in Japanese). *Kenchiku Kenkyu Shiryo*, 6, 33–34.

[31] F. Barda. (1972). Shear strength of low-rise walls with boundary elements. *PhD Thesis/Technical Report, Lehigh University, Bethlehem, PA, USA.*

[32] K. Emori, W.C. Schnobrich. (1978). Analysis of reinforced concrete frame-wall structures for strong motion earthquakes. Report No. UILU-ENG-78-2025 (Structural Research Series No. 457). *University of Illinois Sponsored by National Science Foundation.*

[33] T. Chen, C. Guestrin. (2016). XGBoost: A scalable tree boosting system. *Proceedings of the 22nd ACM SIGKDD International Conference on Knowledge Discovery and Data Mining (pp. 785–794). ACM.* https://doi.org/10.1145/2939672.293978

[34] L. Breiman, J. Friedman, R. Olshen, C. Stone. (1984). Classification and Regression Trees. Chapman and Hall/CRC. https://doi.org/10.1201/9781315139470

[35] T. Hastie, R. Tibshirani, J. Friedman. (2009). The Elements of Statistical Learning: Data Mining, Inference, and Prediction. *Springer*.

[36] L. Breiman. (2001). Random forests. *Machine Learning*, 45, 5–32. https://doi.org/10.1023/A:1010933404324

[37] A. Liaw, M. Wiener. (2002). Classification and regression by randomForest. *R News*, 2(3), 18–22.

[38] F. Pedregosa et al. (2011). Scikit-learn: Machine Learning in Python. *Journal of Machine Learning Research*, 12, 2825-2830.